An Asp–CaM complex is required for centrosome–pole cohesion and centrosome inheritance in neural stem cells

Todd Schoborg, Allison L. Zajac, Carey J. Fagerstrom, Rodrigo X. Guillen, and Nasser M. Rusan

Cell Biology and Physiology Center, National Heart, Lung, and Blood Institute, National Institutes of Health, Bethesda, MD 20892

The interaction between centrosomes and mitotic spindle poles is important for efficient spindle formation, orientation, and cell polarity. However, our understanding of the dynamics of this relationship and implications for tissue homeostasis remains poorly understood. Here we report that *Drosophila melanogaster* calmodulin (CaM) regulates the ability of the microcephaly-associated protein, abnormal spindle (Asp), to cross-link spindle microtubules. Both proteins colocalize on spindles and move toward spindle poles, suggesting that they form a complex. Our binding and structure–function analysis support this hypothesis. Disruption of the Asp–CaM interaction alone leads to unfocused spindle poles and centrosome detachment. This behavior leads to randomly inherited centrosomes after neuroblast division. We further show that spindle polarity is maintained in neuroblasts despite centrosome detachment, with the poles remaining stably associated with the cell cortex. Finally, we provide evidence that CaM is required for Asp's spindle function; however, it is completely dispensable for Asp's role in microcephaly suppression.

Introduction

Faithful chromosome segregation relies on the collective effort of the mitotic spindle and hundreds of macromolecules that regulate its structure, behavior, and function (Walczak and Heald, 2008). In a simplified view, the spindle is a two-component system consisting of microtubules (MTs) and MT-associated proteins. The interplay between these components dictates spindle architecture and harnesses its dynamics to ensure proper ploidy.

A large number of genes play a role in various aspects of spindle biology (Goshima and Vale, 2003; Goshima et al., 2007). Despite this, spindle phenotypes that arise from mutations in these genes fall into a limited number of categories, suggesting that spindle form and function is dictated by only a handful of basic principles. These phenotypes manifest as defects in spindle length and shape, centrosome number and positioning, kinetochore function, and chromosome congression and segregation (Goshima et al., 2007). Some spindle assembly genes have been well studied, providing insight into the mechanism by which they influence the spindle; however, mechanistic insight into most spindle genes remains lacking.

Spindle pole focusing is one example in which many essential genes have been identified with little understanding of how it is achieved. Loss of MT focusing at spindle poles has been documented after perturbation of several MT-associated proteins and motors, including the kinesins Ncd/Kar3 and Eg5 (Sawin et al., 1992; Endow et al., 1994; Gaglio et al., 1996; Matthies et al., 1996) in addition to dynein, dynactin, and nuclear mitotic apparatus protein (NuMA; Merdes et al., 1996). This latter complex is the best understood, primarily because of biochemical data that support a model where NuMA oligomerizes and binds directly to MTs and dynein/dynactin complexes, leading to MT cross-linking and pole focusing (Harborth et al., 1999; Merdes et al., 2000).

In *Drosophila melanogaster*, several nonmotor proteins, such as the kinase regulator Mob4 and the microcephaly-associated protein abnormal spindle (Asp), are required for pole focusing (Ripoll et al., 1985; Wakefield et al., 2001; Trammell et al., 2008), but the mechanism of pole focusing remains less clear. In *Drosophila*, mushroom body defect (Mud) has been suggested to be an ortholog of vertebrate NuMA; however, there is little sequence similarity, and data suggest the primary role of mushroom body defect is to maintain spindle orientation through interaction with the Pins-Gαi cortical polarity proteins (Bowman et al., 2006). Instead, Asp is a more likely candidate as a "functional" ortholog of NuMA given its spindle pole localization, its ability to bind MTs, and phenotypes associated with *asp* mutations, such as centrosome detachment and loss of pole focusing (Gonzalez et al., 1990; Saunders et al., 1997; do Carmo Avides and Glover, 1999; Wakefield et al., 2001; Morales-Mulia and Scholey, 2005). Interestingly, vertebrates possess a true ortholog of *asp*, known as *abnormal spindle-like*

Correspondence to N.M. Rusan: Nasser@nih.gov

Abbreviations used in this paper: Asp, abnormal spindle; ASPM, abnormal spindle-like microcephaly associated; Df, deficiency; FL, full length; GMC, ganglion mother cell; MT, microtubule; NB, neuroblast; NuMA, nuclear mitotic apparatus protein; WT, wild type.

The Rockefeller University Press $30.00
J. Cell Biol. Vol. 211 No. 5 987–998
www.jcb.org/cgi/doi/10.1083/jcb.201509054

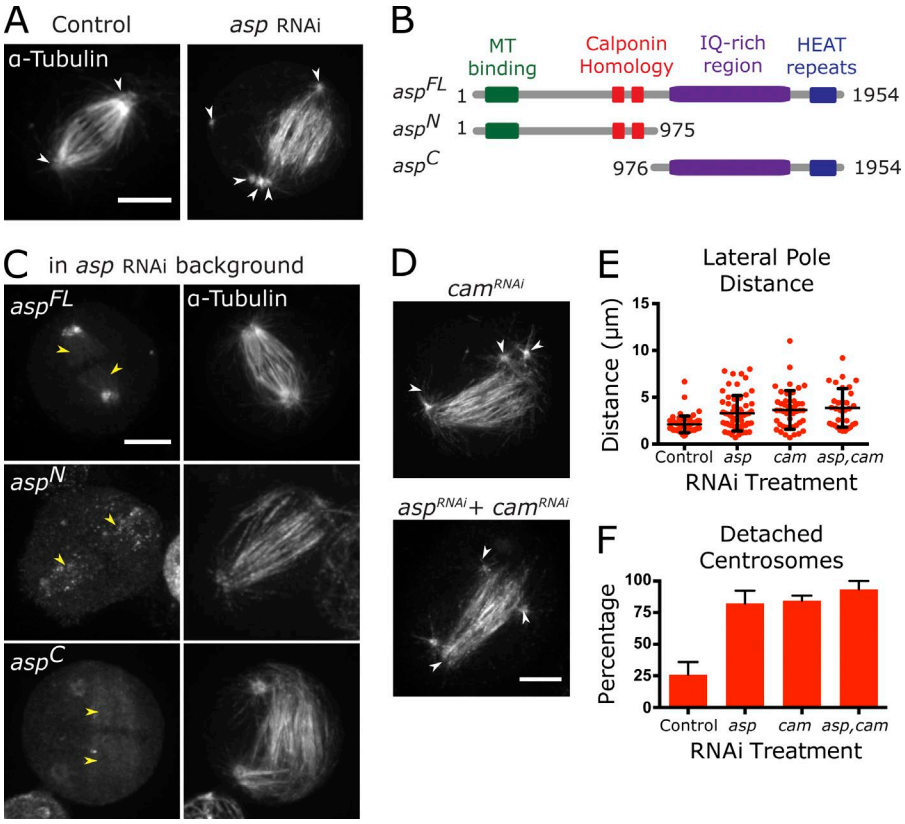

Figure 1. **Asp and CaM are required for pole focusing and centrosome attachment.** (A) Control and *asp* RNAi S2 cells expressing RFP-α-tubulin. Arrowheads indicate centrosomes. (B) Schematic of Asp^{FL}, Asp^{N}, and Asp^{C}, indicating structural domains. (C) GFP-tagged Asp^{FL}, Asp^{N}, or Asp^{C} in S2 cells expressing RFP-α-tubulin and treated with *asp* RNAi. Yellow arrowheads indicate spindle localization of Asp constructs. (D) S2 cell treated with *cam* RNAi or *asp* and *cam* RNAi. Arrowheads indicate centrosomes. (E) Measurement of lateral pole distances for each RNAi treatment ($n > 30$; error bars are SD). (F) Percentage of cells with centrosomes detached from spindle ($n > 15$ cells from three independent experiments; error bars are SD). Bars, 5 µm.

microcephaly associated (*ASPM*), which is the most commonly mutated gene in patients afflicted with autosomal-recessive primary microcephaly, characterized by reduced head and brain size and mental retardation (Bond et al., 2002, 2003). Asp and ASPM play key roles in neural development in both flies and mice (Fish et al., 2006; Rujano et al., 2013). However, the mechanism of Asp and ASPM function remains largely unexplored.

Underlying our deficit in understanding Asp function is the lack of a null allele to afford robust genetic analysis. Here, we use CRISPR, live cell imaging of *Drosophila* neural stem cells (neuroblasts [NBs]), and mutant analysis to investigate the underlying mechanism of Asp regulation. We show that Calmodulin (CaM) forms a complex with Asp that dynamically associates with MTs and regulates its role in centrosome–pole cohesion, pole focusing, and proper centrosome inheritance, but not its role in suppressing microcephaly.

Results

Asp and CaM are required for pole focusing and centrosome attachment

In agreement with previous studies (Morales-Mulia and Scholey, 2005), two prominent spindle phenotypes were observed after RNAi depletion of Asp from cultured S2 cells: unfocused spindle poles and centrosome detachment from spindles (Fig. 1, A, E, and F; and Fig. S1 A). We found centrosomes randomly positioned throughout the cell, and in cells with more than two centrosomes (common in S2 cells), they fail to cluster in mitosis (Fig. 1 A). To probe the underlying molecular basis of these phenotypes, we localized GFP-tagged full length (FL) and truncations of Asp in S2 cells depleted of endogenous Asp (Fig. 1, B and C). FL Asp (Asp^{FL}) rescued pole focusing, centrosome detachment, and unclustering; however, Asp^{N} and Asp^{C} did not (Fig. 1, C, E, and F). Interestingly, in addition to Asp localization to spindle poles, we identified a previously unreported population decorating the entire spindle (Fig. 1 C). This MT localization can be divided into two populations as revealed by Asp truncations: Asp^{N} formed discrete spindle puncta (similar to Asp^{FL}), whereas Asp^{C} localized weakly throughout the spindle, consistent with very weak affinity found in vitro between MTs and $Asp^{621–1196}$ (Saunders et al., 1997), which partially overlaps with our $Asp^{C\ (976–1954)}$. We believe this Asp^{C} localization is normally masked by the stronger spindle pole and punctate localization of wild type (WT). Therefore, our truncation analysis uncovered two modes of MT attachment: (a) punctate attachment, likely mediated by the known MT-binding domain at the N terminus, and (b) a diffuse, weak attachment mediated by an unknown region within Asp^{C}. Importantly, MT localization of either Asp^{N} or Asp^{C} alone is insufficient for Asp function, suggesting proper pole focusing and centrosome attachment require the coregulation of the N and C termini.

Based on our data, we hypothesized that two key domains of Asp are required for its localization and function: the high-affinity MT-biding domain within Asp^{N} and an IQ motif–rich region in Asp^{C} that was computationally identified, yet remains unexplored (Fig. S2 A; Saunders et al., 1997; Franke et al., 2006). Given CaM is known to bind IQ motifs and was shown to be required for pole focusing (Goshima et al., 2007), we hypothesized that CaM directly binds and regulates Asp. In support of this, RNAi depletion of *cam* in S2 cells phenocopied *asp* depletion in our measurements (Fig. 1, D–F; and Fig. S1 A). Similar phenotypes were also observed on acute drug treatment of S2 cells using W-7, a cell-permeable CaM inhibitor (Fig. S1 B; Osawa et al., 1998). Furthermore, depletion of both *asp* and *cam* simultaneously did not lead to a more severe phenotype

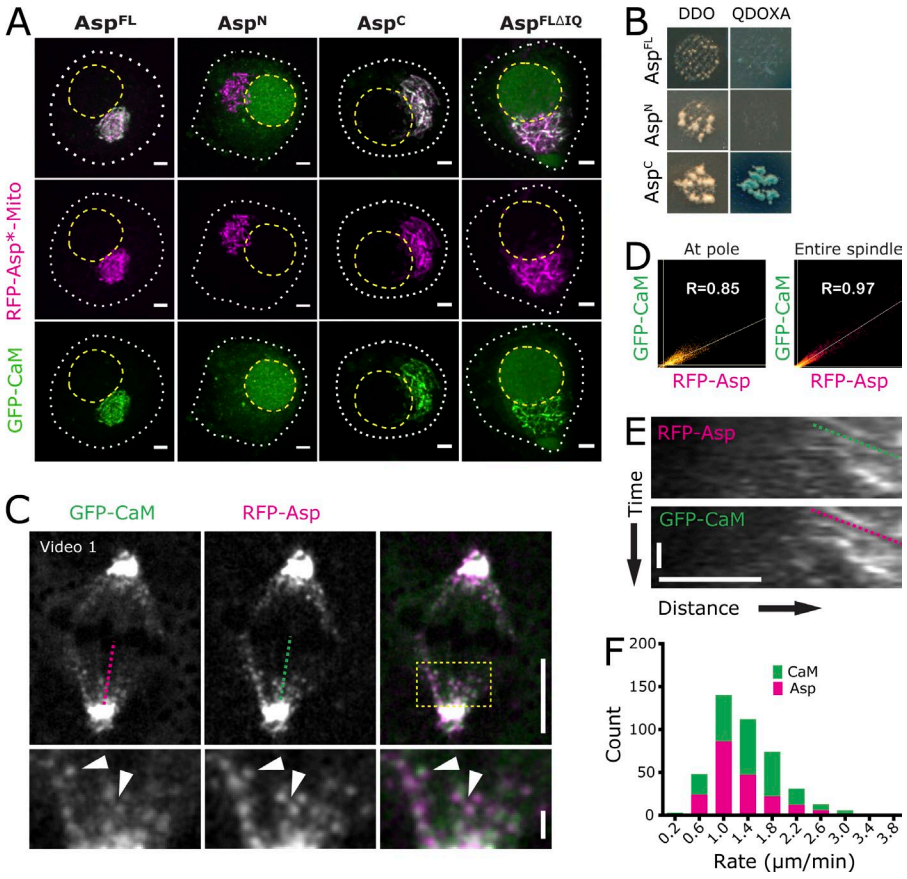

Figure 2. **Asp and CaM interact to form a complex that streams along spindles.** (A) Mitochondria targeting assay for each of the indicated Asp fragments. White dotted line corresponds to cell outline, and yellow dotted lines show nuclei. Bar, 2 µm. (B) Yeast two-hybrid analysis of Asp constructs and CaM. Left column indicates growth, and right column indicates interaction. (C) Single frame from Video 1 of live S2 cell expressing RFP-CaM and GFP-Asp. Boxed region (yellow) denotes inset, bottom panel. Colored lines represent position of kymograph in E. Arrowheads denote colocalized foci. Bar, 5 µm; inset, 1 µm. (D) 2D histograms from colocalization analysis. (E) Kymograph along positions denoted in C. Time bar, 1 min; distance bar, 2.5 µm. (F) Histogram of movement rates for CaM and Asp (µm/min). $n > 200$ tracks from more than nine cells.

(Fig. 1, E and F), suggesting both function in the same genetic pathway, possibly as a complex.

To test if loss of pole focusing is a consequence of centrosome detachment, we repeated our knockdown in cultured cells lacking centrosomes (*sas4*$^{-/-}$; Lecland et al., 2013). Loss of *asp*, *cam*, or both led to a significant increase in lateral pole distance (Fig. S1, C–E). This is in agreement with previous work that showed poles are focused in centrosome-less *asl*^{2} mutant NBs and unfocused in the *asl*^{2},*asp*^{1} double mutant (Wakefield et al., 2001). These results suggest that CaM and Asp cooperate to perform two independent roles at spindle poles: MT focusing and centrosome–pole attachment. However, these two roles are likely mediated by the same lateral MT–MT interaction mechanism.

Asp and CaM interact and display identical dynamics

To test if Asp and CaM form a complex in vivo, we used a mitochondria targeting assay, which uses colocalization to assess the interaction between two proteins expressed off the same plasmid after the artificial tethering of one to the mitochondria (Galletta et al., 2014). In addition to Asp^{FL}, Asp^{N}, and Asp^{C}, we generated a FL construct in which five highly predicted IQ motifs in the C terminus were deleted (Asp$^{FL\Delta IQ}$; Fig. S2 A; Franke et al., 2006). In this assay, CaM interacted strongly with Asp^{FL} and Asp^{C}, but not with Asp^{N} (CaM remained exclusively nuclear). Interestingly, the Asp$^{FL\Delta IQ}$ construct was still able to bind CaM, but this interaction was reduced as evident by its inability to pull most of CaM out of the nucleus (Fig. 2 A). This suggests that other predicted IQ motifs in the C terminus of Asp (Rujano et al., 2013) contribute to CaM binding. Nevertheless, our phenotypic analysis (see Fig. 5) indicates the perturbation of CaM interaction in Asp$^{FL\Delta IQ}$ is significant. We verified that the Asp^{C}–CaM interaction is direct using yeast two-hybrid analysis (Galletta and Rusan, 2015), in agreement with previous Asp-CaM Y2H analysis in *Caenorhabditis elegans* (van der Voet et al., 2009). However, unlike the mitochondrial targeting assay, an interaction with CaM was only revealed on separating the N and C termini (Fig. 2 B). This suggests that the Asp^{FL}–CaM interaction requires a specific Asp tertiary structure only afforded in *Drosophila* cells.

To further validate Asp–CaM interactions in a physiologic context, we simultaneously imaged RFP-CaM and GFP-Asp on mitotic spindles in S2 cells. Both proteins localized in a near identical pattern with strong enrichment at spindle poles and weaker foci throughout the spindle (Fig. 2, C and D). Remarkably, live imaging revealed that Asp and CaM foci moved concertedly poleward along the metaphase spindle at similar velocities (Asp: 1.3 ± 0.5 µm/min; CaM: 1.5 ± 0.6 µm/min), gradually accumulating at the poles (Fig. 2, E and F; and Video 1). The concomitant movement of Asp and CaM toward the poles argues these proteins are organized as a complex. Furthermore, the similarity of their velocities to MT flux in S2 cells (1.1–1.2 µm/min; Matos et al., 2009; Rath et al., 2009) suggests these complexes bind MTs directly and not through a minus end motor traveling along the MT.

CaM is required to stabilize Asp^{C}, which can form higher-order structures with Asp^{FL}

Evidence in vertebrates suggests NuMA can oligomerize, generating an insoluble pole matrix that facilitates focusing

(Dionne et al., 1999; Harborth et al., 1999; Merdes et al., 2000). We hypothesized that Asp might mediate pole focusing in *Drosophila* using an analogous mechanism, with CaM acting as the lynchpin. We used our mitochondria targeting assay and cotransfected FLAG-tagged versions of Asp^{FL}, $Asp^{FL\Delta IQ}$, Asp^{N}, and Asp^{C} and found that the Asp^{C} fragment could interact with both Asp^{FL} and $Asp^{FL\Delta IQ}$. We did not observe an interaction with Asp^{C} or Asp^{N} (Fig. S2 B). Although the Asp^{C}-$Asp^{FL\Delta IQ}$ suggest otherwise, it is still possible that CaM is required for this interaction by binding the five major IQ motifs in Asp^{C}, or binding the other nonmajor IQ motifs that remain in $Asp^{FL\Delta IQ}$. We attempted to investigate this further by depleting CaM using RNAi in the aforementioned assay; unfortunately, Asp^{C} was not detected in cells (Fig. S2 C), suggesting CaM is required for Asp^{C} stability. Therefore, our data show that Asp canoligomerize in vivo via its C terminus, but the interaction appears to require a structural feature present within the FL protein, and it remains to be determined if CaM is required for this interaction.

The failure to detect the Asp^{C} fragment after CaM depletion suggested that CaM might regulate Asp behavior through stabilization of Asp protein. We tested this hypothesis by expressing CaM-GFP and Asp^{FL}-FLAG constructs in S2 cells treated with control or CaM RNAi. We were unable to quantify Asp^{FL}-FLAG stability via Western blotting because of our inability to obtain a reproducible migrating band on SDS-PAGE gels from these extracts. We therefore quantified the percentage of cells expressing Asp^{FL}-FLAG using immunostaining and found a significant decrease in the number of interphase cells expressing Asp^{FL}-FLAG after CaM depletion (Fig. S2 D). These data suggest that a potential mechanism of Asp regulation by CaM involves protein stability; however, more biochemical analysis will be required to verify and extend these findings, particularly within the spindle lattice itself.

CaM and Asp dynamics in NBs

Asp and its vertebrate orthologue ASPM are key determinants of neural development (Bond et al., 2002, 2003; Fish et al., 2006; Rujano et al., 2013), providing a relevant system to probe the role of the Asp–CaM interaction in the context of a developing tissue. To begin, we analyzed endogenous CaM localization by immunostaining *Drosophila* larval central NBs (Morin et al., 2001), which undergo repeated rounds of rapid asymmetric cell divisions. Our fixed analysis of prophase NBs shows CaM distinctly localized to the centrosomes (Fig. 3, A and A′). During metaphase, CaM redistributed proximally from the centrosomes to the spindle pole region, with smaller punctae throughout the spindle (Fig. 3, B and B′). Similar CaM localization on spindles was observed in mitotic S2 cells overexpressing GFP-CaM (Fig. S3). To gain further insight into the dynamic behavior of these two spindle populations of CaM in NBs, we used live-cell imaging. Metaphase NBs show endogenous CaM streaming within the spindle, leading to incorporation into a pool of immobilized CaM at the poles (Fig. 3, C and D′). This streaming behavior ceases during late anaphase as the chromosomes separate (Videos 2 and 3). Critically, we observed identical dynamics of Asp^{FL} in NBs (Video 4), consistent with a pole focusing mechanism that relies on Asp–CaM complexes. Finally, by telophase, CaM localizes near the cleavage furrow (Fig. 3, C and C′; and Video 2), suggesting that CaM also plays an important role in Asp's function during cytokinesis (Wakefield et al., 2001; Riparbelli et al., 2002), possibly aiding the cross-linking and stabilization of midbody MT minus ends.

Asp null mutations cause spindle defects in NBs

Previous research was conducted using hypomorphic *asp* alleles (Gonzalez et al., 1990), which may confound genetic analysis and functional studies. We used CRISPR to generate a null *asp* allele (asp^{t25}) by excising an ∼750-bp fragment of the *asp* locus that includes the promoter, proximal regulatory elements, 5′ UTR, and the first exon (Fig. 4, A and B). *asp* transcription was completely abolished in transheterozygote animals carrying the asp^{t25} and a deficiency (*Df*) that removes the *asp* locus (Fig. 4 C), indicating that asp^{t25} is a null allele. All subsequent experiments, unless noted, were performed in the asp^{t25}/*Df* background, hereafter referred to as asp^{t25}. These adult flies are viable but sterile with small heads (Fig. 4 D), similar to the microcephaly phenotype previously documented for hypomorphic alleles (Gonzalez et al., 1990; Rujano et al., 2013). Importantly, asp^{t25} mutant NBs exhibited complete loss of CaM recruitment to spindles, unfocused spindle poles, and detached centrosomes (Fig. 4 E). Identical phenotypes were also observed in asp^{t25} homozygotes, further confirming asp^{t25} is a null allele and providing a powerful tool for determining the link between spindle behavior and tissue homeostasis.

To test the importance of the Asp–CaM interaction in vivo, we generated transgenic animals expressing GFP-tagged versions of asp^{FL}, asp^{N}, asp^{C}, and $asp^{FL\Delta IQ}$ in the asp^{t25} mutant background and analyzed their effect on spindle morphology and head size. Although asp^{FL} fully rescued the mutant spindle phenotypes, asp^{N}, asp^{C}, and $asp^{FL\Delta IQ}$ did not; rather, they resulted in curved, unfocused spindles and detached centrosomes, indistinguishable from asp^{t25} mutants (Fig. 5 A). Asp^{FL}, Asp^{N}, and $Asp^{FL\Delta IQ}$ proteins localized to spindle poles and discrete puncta within the spindle, whereas Asp^{C} showed a weak spindle localization visible in live NBs (Fig. 5 B) that was lost in fixed preparations (Fig. 5 A). Our live analysis further revealed that Asp^{N} and $Asp^{FL\Delta IQ}$ retain the ability to stream toward the poles (Video 4), indicating that CaM–Asp complexes are required for the lateral MT–MT interactions that support spindle pole focusing, but they are not required for the N terminus of Asp to bind MT minus ends.

Previous work has shown various *asp* allelic combinations lead to small fly brains, similar to human microcephaly (Rujano et al., 2013). We also found asp^{t25} and asp^{C} adults with significant brain size reduction; conversely, $asp^{FL\Delta IQ}$ (reduced CaM interactions) and asp^{N} (no CaM interaction) rescued brain size comparable with asp^{FL} and WT animals (Fig. 6). Therefore, CaM is required for Asp's spindle assembly role, but not its role in microcephaly suppression.

Centrosome inheritance in NBs is randomized in *asp* mutants

Maintaining centrosome–pole attachment is an intriguing, yet underappreciated function for Asp and CaM. Previous studies have noted this phenotype for other *asp* alleles in the embryo and brain (Gonzalez et al., 1990; Wakefield et al., 2001); however, the mechanism of detachment and its consequences have not been explored. To this end, we used live imaging of GFP-Tubulin to monitor centrosome and spindle dynamics in asp^{t25} mutant NBs. Early stages of mitosis, including events up to and including NEB proceeded normally, similar to WT NBs (Fig. 7, A and B). Shortly after NEB, centrosomes detach from the poles and move randomly around the cell (Fig. 7, B and C; and Videos 5–8). Polarity establishment in these NBs

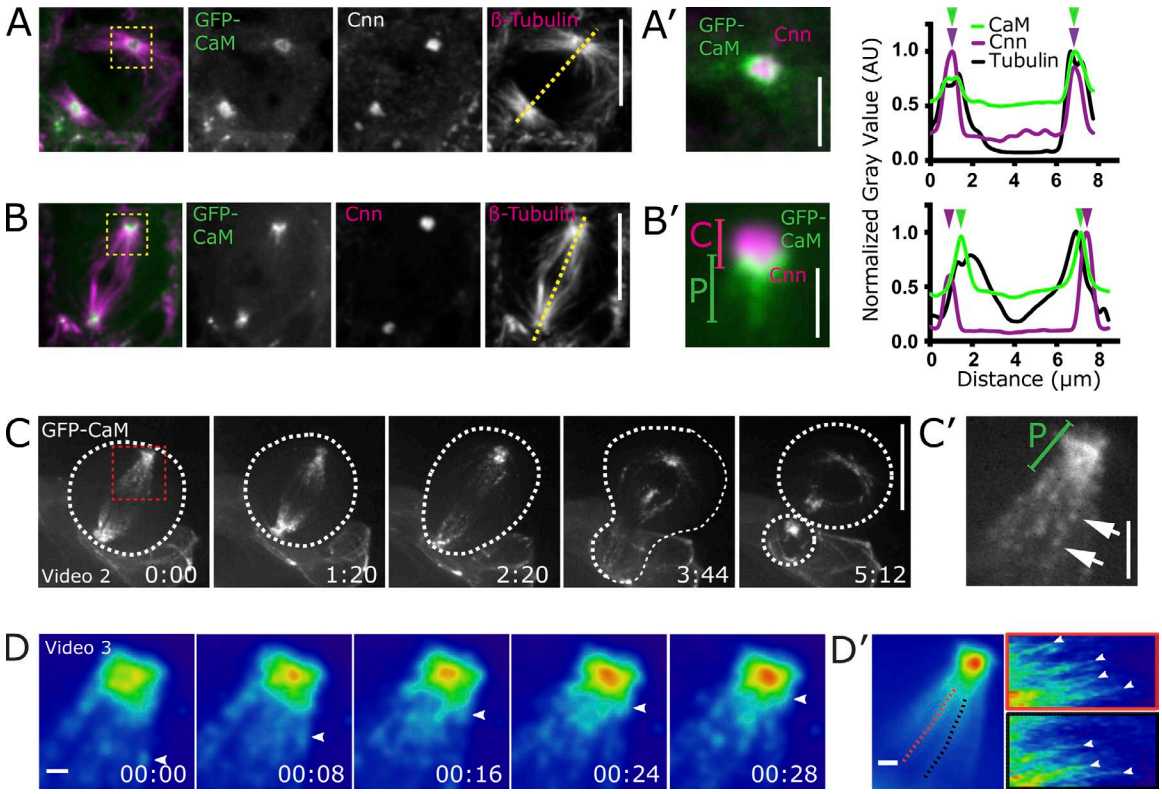

Figure 3. **CaM localization and dynamics in NBs.** (A) Prophase NBs from larvae expressing GFP-CaM stained for centrosomin (Cnn) and β-tubulin. (A′) Close up of yellow boxed region in A and line scan along the yellow line for CaM, Cnn, and Tubulin. (B) As described for A, but the cell is in metaphase. (B′) As described for A′. Note the difference in CaM localization relative to the centrosome between prophase (A) and metaphase (B). C, centrosome; P, pole. (C) Live cell imaging of mitotic NB (dotted outline) expressing GFP-CaM (Video 2). (C′) Inset of red boxed region in C. Arrows denote spindle foci. P, pole. (D) Still frames from metaphase NB (Video 3), with arrowhead denoting GFP-CaM foci moving toward the pole. Note the increase in signal intensity at pole as time progresses. (D′) Average intensity projection of metaphase (left panel) showing position of kymographs (right). Arrowheads denote foci movement. Bars: (A and B) 5 μm; (A′ and B′) 1 μm; (C) 10 μm; (C′, D, and D′) 2 μm.

was not impaired, consistent with early mitotic events being normal in *asp*^{t25} mutants. Even more interesting is that cell polarity was maintained through mitosis and was always associated with spindle poles, not the wandering centrosomes (Fig. 7 D and Fig. S4 A).

We followed NBs as they exited mitosis to determine the fate of the nomadic centrosomes and found that their location at anaphase onset determined inheritance. We observed instances in which mother and daughter centrosomes were correctly inherited (Fig. S4, B and B′; and Video 5) and others in which they swapped positions before segregation (Fig. 7, C and C′; and Video 7). Previous work has highlighted asymmetry in composition and function between the mother and daughter centrosomes, with NBs retaining the daughter and ganglion mother cells (GMCs) inheriting the mother (Rebollo et al., 2007; Rusan and Peifer, 2007; Conduit and Raff, 2010; Januschke et al., 2011, 2013; Lerit and Rusan, 2013). Although the purpose of this asymmetry remains unclear (Lerit et al., 2013), our *asp*^{t25} mutant provides an excellent model for testing such questions. Additionally, we observed cases where both centrosomes were inherited by the NB (Fig. 7, B and B′; and Video 6) or the GMC (Fig. S4, C and C′; and Video 8).

Given these defects, we predicted that the duration of mitosis would increase. Indeed, we find many *asp*^{t25} NBs with extended metaphase duration (Fig. 7, B and C; and Fig. S4 C), whereas others proceed with near WT timing (Fig. S4 B). Importantly, we did not observe any cases of complete mitotic arrest in NBs as determined by our living imaging and mitotic index analysis (Fig. S4 D), in contrast with previous studies for other *asp* alleles (Ripoll et al., 1985; Carmena et al., 1991; Wakefield et al., 2001). It is not clear why a longer metaphase does not lead to an increase in mitotic index, but it is not because of a change in NBs numbers (Fig. S4 E), suggesting that the entire NB cell cycle is extended, not just metaphase. Nevertheless, the downstream consequence of receiving too many or too few centrosomes are well documented, including chromosome instability, tumor formation, and cell death (Basto et al., 2006; Rusan and Peifer, 2007; Castellanos et al., 2008; Lerit and Rusan, 2013; Sir et al., 2013; Poulton et al., 2014).

Discussion

The results presented here provide insight into how Asp, a key protein involved in mitotic spindle function, is regulated by the ubiquitous calcium-sensing protein CaM. CaM was localized near the spindle poles over 35 yr ago (Welsh et al., 1978); our data now assign a role for this CaM localization in directly regulating Asp to cross-link spindle MTs. The Asp-CaM interaction is conserved because it has also been biochemically identified in other eukaryotes, such as nematodes and mice, suggesting that this complex performs an essential spindle function (van der Voet et al., 2009; Xu et al., 2012). The work presented here extends our functional understanding of the Asp–CaM complex

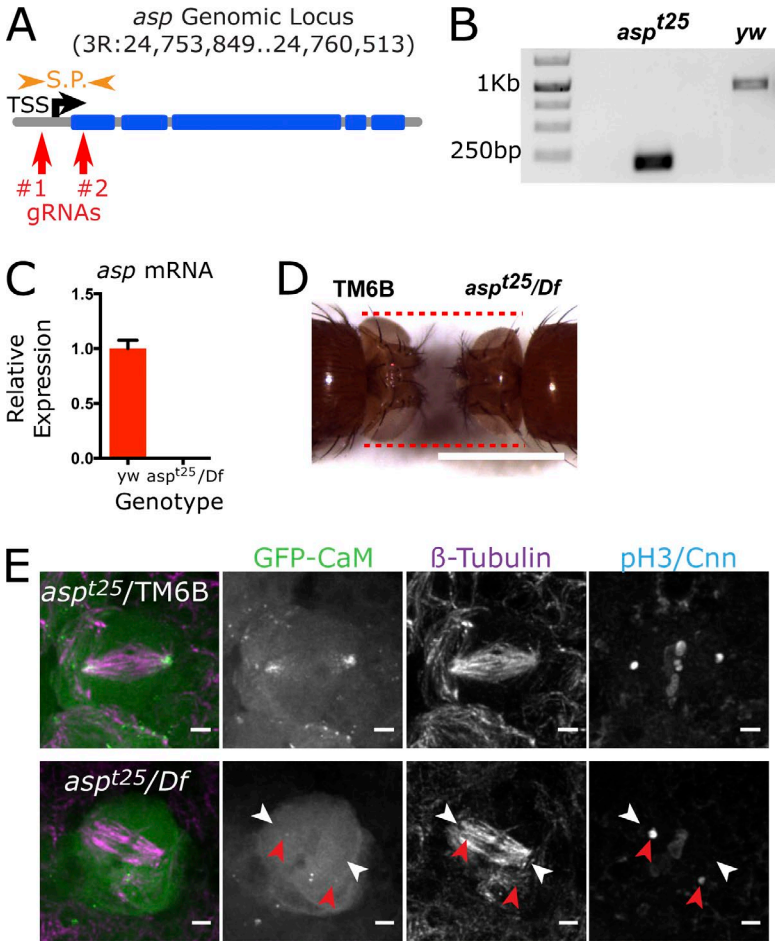

Figure 4. **Generating *asp* null allele using CRISPR.** (A) Schematic of the *asp* locus and region targeted for deletion. Position of guide RNAs (red arrows) and primers used for PCR screening (orange arrows; S.P., sequence primers). TSS, transcriptional start site. (B) PCR screen from control (*yw*) and asp^{t25}/Df flies. (C) Quantitative PCR of *asp* transcript levels (three biological replicates, error bars are SEM). (D) Head size in age-matched control (TM6B) and asp^{t25}/Df adults. (E) NBs from control (top panel, asp^{t25}/TM6B) and asp^{t25}/Df (bottom panel) mutant larvae expressing GFP-CaM and stained for β-tubulin, pH3, and centrosomin (Cnn). White arrowheads denote pole position and red arrowheads denote centrosome position. Bars: (D) 1 mm; (E) 2 µm.

in spindle pole focusing and centrosome–pole cohesion, in addition to the cell biology of microcephaly.

Previous work in *Drosophila*, *C. elegans*, and mice has suggested a link between Asp and CaM. Goshima et al. (2007) were first to highlight the similar spindle phenotypes observed after RNAi depletion of either protein in *Drosophila* S2 cells. In *C. elegans*, analysis of meiotic spindles in the early embryo showed spindle defects after *asp* depletion and Asp's dependence on CaM (CMD-1) for pole localization. Furthermore, yeast two-hybrid analysis identified an Asp fragment containing a single IQ motif that could interact with CMD-1 (van der Voet et al., 2009). This interaction between CaM and Asp on meiotic spindles was later identified in mouse oocytes using immunoprecipitation (Xu et al., 2012). However, in all cases, details of the underlying mechanism of the Asp–CaM association and a direct test of its contribution to spindle architecture remained unexplored.

Our results demonstrate that CaM functions as the critical factor that dictates Asp's ability to cross-link MTs. This is supported by the fact that Asp transgenes that localize to the spindle in a manner identical to that of the FL protein, yet are defective in CaM binding (Asp^{N} and $Asp^{FL\Delta IQ}$), fail to maintain pole focusing and centrosome–pole cohesion. Further, our transgene analysis also highlighted a second mode of MT binding by Asp, mediated through its C terminus, and is independent of its known N-terminal MT binding domain. This interaction, though clearly weaker and distinct from the punctate signals observed for N-terminal containing transgenes, is supported by previous studies in vitro (Saunders et al., 1997). We believe the stronger spindle pole and punctate localization of WT Asp normally masks this Asp^{C} localization and possibly contributes to Asp's ability to cross-link MTs (see model in Fig. 8).

Furthermore, we also uncovered a novel mode of Asp–CaM complex behavior on spindles, highlighted by dynamic streaming of foci through the spindle lattice toward the pole. Previous work suggested that Asp associates with MT minus ends based on its accumulation at spindle poles where their density is highest (do Carmo Avides and Glover, 1999; Wakefield et al., 2001). Our localization of the Asp–Cam complex in live cells supports this hypothesis. However, we further suggest that Asp–CaM complexes, seen as discrete puncta that move poleward, reside at MT minus ends distributed throughout the spindle that are collectively transported and organized at poles. These observations are consistent with work showing γ-tubulin–marked minus ends present throughout the spindle that stream toward the poles (Lecland and Lüders, 2014). Additionally, vertebrate NuMA displays similar streaming behavior (Kisurina-Evgenieva et al., 2004), indicating a shared mechanism in which pole focusing is achieved through the concerted movement of protein complexes along the spindle toward the pole. Biochemical analysis will be critical for establishing the relationship between the distribution of minus ends within the spindle, the ability of the Asp–CaM complex to bind MT minus ends, and how the dynamic nature of their movement contribute to pole focusing and centrosome–pole cohesion.

The complete detachment of centrosomes from the spindle and random movement within the NB could have substantial long-term effects that are not fully appreciated by our limited

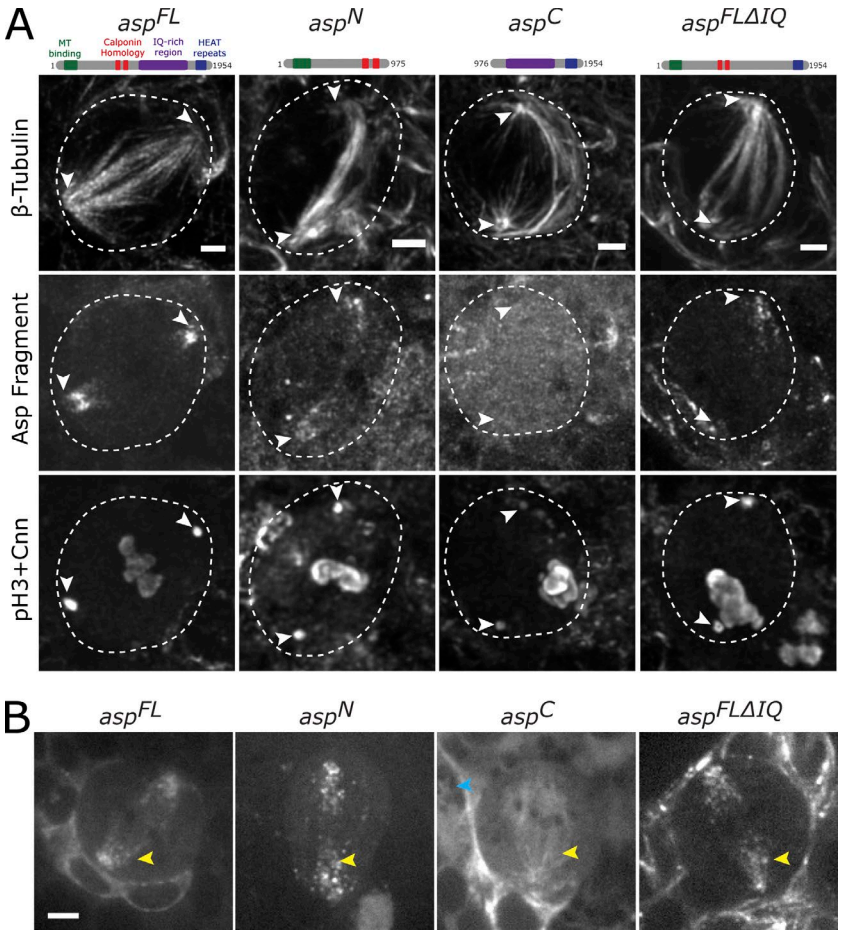

Figure 5. **Analysis of spindles and Asp localization in NBs.** (A) *asp*^{t25}*/Df* NBs expressing indicated transgenes were fixed and stained for β-Tubulin, pH3, and centrosomin (Cnn). Outline denotes NB cortex, and arrowheads mark centrosome position. (B) Snapshots from live movie of indicated genotype. Localization of Asp is similar to samples in A, except here the weak Asp^{C} localization to spindle MTs is clear (yellow arrowheads). Bars, 2 µm.

analysis of third-instar larval brains. Although the swapping of mother–daughter centrosome position and improper inheritance is interesting, its significance is unknown (Lerit et al., 2013). It could be that centrosome position after detachment, rather than detachment, per se, negatively influences mitotic events. One would predict, for example, that centrosomes positioned anywhere in the cell other than the poles could influence the MT architecture within the spindle. In fact, we do see a significant number of aberrantly bent spindles, and our live imaging showed that wandering centrosomes transiently interact laterally along the entire length of the spindle. One might also predict that this lateral centrosome position would influence the dynamics and tension across the kinetochores, triggering the spindle assembly checkpoint and an extended metaphase, which we also document in *asp*^{t25} mutants. Therefore, the wandering centrosomes and their improper inheritance could have many negative downstream effects. If these results of inheriting too many or too few centrosomes are extrapolated to mammalian cells, one would predict detrimental effects on cilia formation in addition to mitotic defects, as previously documented in other mutant backgrounds (Mahjoub and Stearns, 2012).

Our analysis of apical determinants in NBs highlighted a possible role for spindle poles (not centrosomes) in the maintenance of cell polarity. Despite centrosome detachment in the

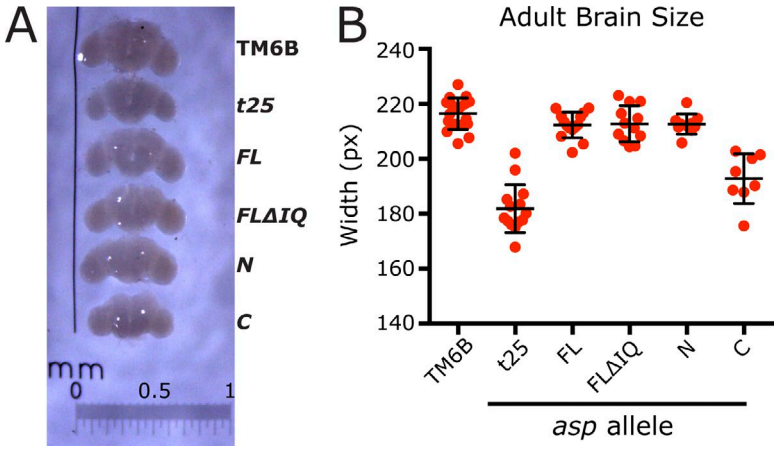

Figure 6. **Analysis of microcephaly phenotypes in *asp*^{t25} *mutants.*** (A) Fixed adult brains from the indicated genotype. (B) Quantitative analysis of head size from A ($n > 8$; error bars are SD). Bar, 1 mm.

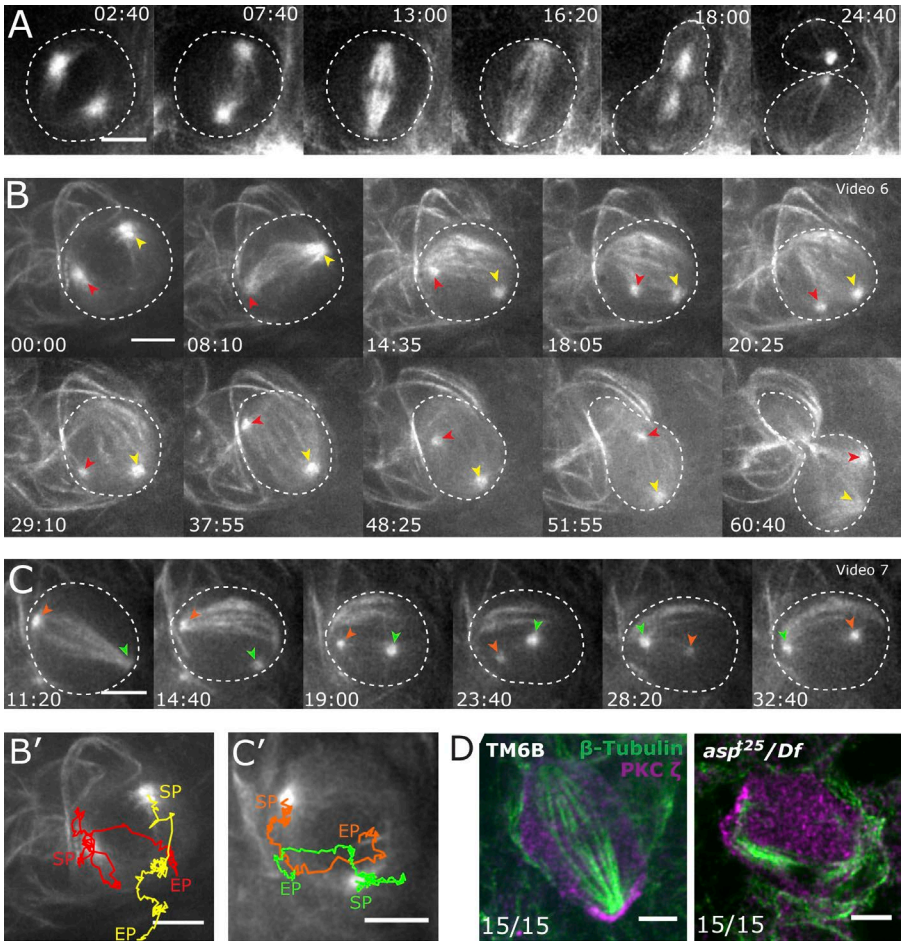

Figure 7. **Centrosome inheritance is randomized in *asp* NBs.** Live imaging of WT (A) and *asp*^{t25}*/Df* mutant (B and C) NBs (dotted outline) expressing GFP-tubulin. (B) Colored arrowheads differentiate and mark positions of the two centrosomes; both are inherited by the NB after asymmetric division. Tracks of centrosome trajectory are shown in B′. (C) An example of mother–daughter centrosome swap. Tracks of centrosome trajectories are shown in C′. (D) Central brain NBs stained with the polarity marker aPKC (PKC ζ; magenta) and β-tubulin (green). *n* = 15 NBs for each phenotype were scored for spindle alignment; a pole touching/oriented toward the aPKC crescent was considered to be properly oriented. EP, end point; SP, start point at prophase. Bars: (A–C) 5 µm; (D) 3 µm.

asp^{t25}*/Df* NBs and long curving spindles, we did not observe misaligned spindles. This was true in fixed tissue using the apical polarity marker aPKC, in which, despite pole splaying and curvature, minus ends of MTs appeared to remain stably associated with the crescent at the cell cortex. Furthermore, we never observed significant spindle rotation after centrosome detachment during the course of live imaging, and NBs divided asymmetrically. These observations support the prevalent model that centrosomes initiate NB polarity (Siegrist and Doe, 2006; Januschke and Gonzalez, 2010) but further add that centrosomes are neither necessary nor able to alter polarity once established. This is corroborated by the fact that we did not observe a significant difference in NB number in the *asp*^{t25}*/Df* mutant, suggesting that cell fate determinants were correctly partitioned during asymmetric division.

Our results also shed light on the role of Asp in microcephaly (Bond et al., 2002). Interestingly, this phenotype is not dependent on the Asp–CaM complex. Both Asp^{N} and Asp$^{FL\Delta IQ}$ rescued the brain size defects of the *asp*^{t25}*/Df* despite showing no or reduced binding to CaM. These results are in agreement with previous work from the Basto laboratory that demonstrated normal head size in animals expressing an N-terminal Asp fragment in the hypomorphic *asp* allele background (Rujano et al., 2013). Importantly, our data using the null allele show that microcephaly is a result of the loss of Asp function and not a dominant-negative effect of the hypomorphic *asp* alleles. Furthermore, we show that the microcephaly phenotype is not a consequence of unfocused spindle poles or detached centrosomes, because the Asp^{N} and Asp$^{FL\Delta IQ}$ rescue fragments displayed both of these defects. Taken collectively, our analysis of the null *asp* allele uncovered a separation of function that requires both termini of Asp to maintain MT cross-linking and an unknown region of the N terminus to specify proper brain size.

In closing, we propose two possible models by which the Asp–CaM complex could function (Fig. 8). In both models, CaM exerts its influence on the spindle through directly binding the C terminus of Asp and is required for its stability. The first model proposes that CaM aids Asp oligomerization within the spindle. Putative higher-order Asp assemblies would be analogous to NuMA oligomerization shown to facilitate MT focusing in vertebrate cells (Dionne et al., 1999; Harborth et al., 1999; Merdes et al., 2000). A second model proposes that CaM might regulate the weak association of Asp's C terminus to MTs. In this model, Asp would bind MT minus ends via its N terminus and the MT lattice via its C terminus, effectively bridging and zippering MTs. In both models, CaM might promote a structural conformation that allows for oligomerization or for a single Asp molecule to bind two separate MTs. Both models are not mutually exclusive, because elements of each may cooperate to ensure proper cross-linking between spindle MTs and centrosome MTs for robust pole focusing and centrosome attachment. Future biochemical and structural studies will be required to more fully understand the influence of CaM binding to Asp and the role of this complex in spindle MT cross-linking.

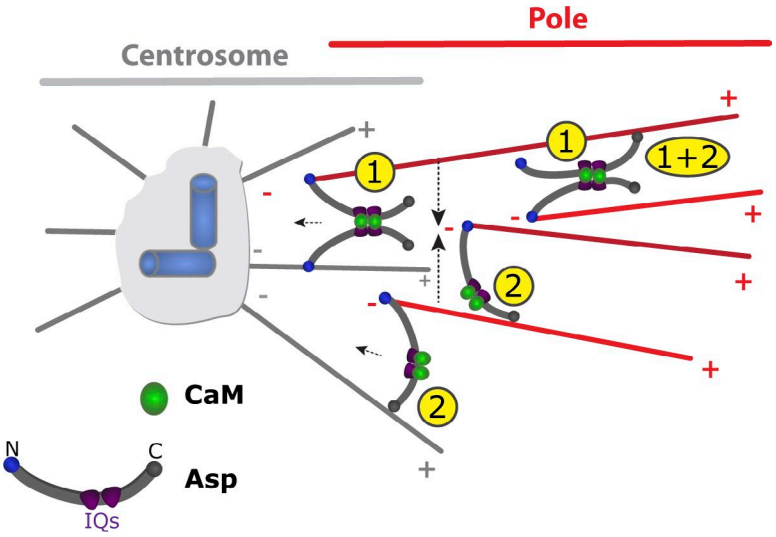

Figure 8. **Model of CaM's possible role in Asp function.** (1) CaM might mediate oligomerization of Asp to cross-link MTs, or (2) CaM might regulate Asp C-terminal interaction with MTs, a mechanism that would provide the necessary MT cross-links for both pole focusing and centrosome attachment.

Materials and methods

Fly stocks and husbandry

All stocks and crosses were maintained on standard cornmeal-agar media at room temperature (20–22°C). The following lines were obtained from the Bloomington Stock Center: w^{1118}; *Df(3R)BSC519/TM6C,* Sb^1 cu^1 (*asp* deficiency mutant, stock 25023); *w*; PPTT-unCamP00695/CyO* (CaM-GFP Trap Line, stock 50843). Microinjection of Asp^{FL}, Asp^{N}, Asp^{C}, and $Asp^{\Delta IQ}$ transgenes into *yw* embryos was performed by BestGene Inc.

Asp CRISPR

Two guide RNAs flanking the *asp* promoter (gRNA1-3R:24753685 ..24753707) and part of the second exon (gRNA2-3R:24754455 ..24754477) were cloned into separate U6 plasmids (pU6-Bbsl). Equimolar amounts (250 ng/µl final) were injected into Cas9 embryos (NIG-FLY CAS-0004) by BestGene Inc. Individual lines were double balanced and progeny screened for small adult head size as homozygotes.

Vectors

For S2 cell expression, modified Gateway cassette vectors from the *Drosophila* Gateway Vector Collection were used to generate GFP (pAGW)-, RFP (pATRW)-, or FLAG-HA (pAFHW)–tagged N-terminal constructs under control of the constitutive Actin5c promoter. CaM stability in these vectors was enhanced by the addition of a 40–amino acid N-terminal linker (GFP-40aaLinker-CaM), which was cloned from an unpublished vector that was a gift from T. Megraw (Florida State University, Tallahassee, FL). To generate the vector for the mitochondria targeting assay, the pAGW vector was digested with *Stu*I and *Age*I to remove the sequence for GFP. A TagRFP cassette containing the N-terminal 36 amino acids of the *Drosophila tom20* gene (gift of H. Xu, National Heart, Lung, and Blood Institute, Bethesda, MD) was PCR amplified and ligated into the *StuI-AgeI* cut site to generate the new destination vector pAT20TRW. The GFP-40aaLinker-CaM and Actin5c promoter were then amplified and inserted into the *Mlu*I site of pAT20TRWto generate pAT20TRW-AGFP-CaM. Asp fragments were then introduced into this vector by standard Gateway cloning. For P-element transformation, a modified pCasper4 cassette (pUGW) containing 5′ and 3′ P-element ends, an *attB* site, and an ubiquitin promoter was used.

Asp constructs and prediction of putative IQ motifs

Five *asp* constructs were generated pertaining to the FL version of the protein (Asp^{FL}, aa 1–1,954), the N-terminal half (Asp^{N}, aa 1–975), the C-terminal half (Asp^{C}, aa 976–1,954), and a FL version lacking five of the most highly predicted IQ motifs ($Asp^{FL\Delta IQ}$): IQ 1 (aa 1,011–1,041), IQ 2 (aa 1,087–1,103), IQ 3 (aa 1,329–1,342), IQ 4 (aa 1,528–1,550), and IQ 5 (aa 1,719–1,731). IQ motif predictions were performed with the FL *Drosophila* Asp protein using the Calmodulin Target Database using default settings.

Yeast two-hybrid

Asp constructs and CaM were introduced into pDEST-pGADT7 and pDEST-pGBKT7 (Rossignol et al., 2007) using the Gateway cloning system (Life Technologies). Before use in cloning, the kanamycin resistance cassette in pDEST-pGBKT7 was replaced with an ampicillin resistance cassette using yeast-mediated recombination. Fragments in pGADT7 or pGBKT7 were transformed into yeast strains Y187 and Y2HGold, respectively (Clontech) using standard techniques. Cultures of yeast carrying these plasmids were grown to OD_{600} ~0.5 at 30°C in SD Leu or SD –Trp media as appropriate to maintain plasmid selection. For mating, 20 µl of a Y187 strain and a Y2HGold strain were added to 100 µl of 2× yeast extract/peptone/dextrose medium in the well of a 96-well plate. Mating cultures were grown for 20–24 h at 30°C with shaking. Approximately 3 µl of cells were then pinned onto SD –Leu –Trp (DDO) plates using a Multi-Blot Replicator (VP 407AH; V&P Scientific), and plates were grown for 5 d at 30°C. These plates were replica plated onto four plates: (a) DDO, (b) QDO (SD –ade –leu –trp –ura), (c) DDOXA (SD –leu –trp plates containing Aureobasidin A; Clontech) and X-α-Gal (Gold Biotechnology), and (d) QDOXA (SD –ade –leu –trp –ura with Aureobasidin A and X-α-Gal). Plates were grown for 5 d at 30°C. Interactions were scored based on growth and development of blue color as appropriate.

Cell culture, transfection, and double stranded RNA treatment

Drosophila S2 cells were obtained from Life Technologies and maintained in SF900 insect media supplemented with 1× penicillin/streptomycin at 25°C. The acentriolar *dSas4-; Jupiter::GFP* cells (Line 131; Lecland et al., 2013) were obtained from the *Drosophila* Genomic Resource Center and maintained in SF900 containing 1× P/S and 5% FBS. Transfection of S2 cells was achieved using Amaxa Nucleofector technology (Lonza). 2 µg vector was diluted in 100 µl nucleofection solution (50 mM D-mannitol, 15 mM $MgCl_2$, 5 mM KCl, and 120 mM $NaPO_4$, pH 7.2) and used to resuspend a pellet of ~4 × 10^6 cells. This

solution was added to a cuvette and electroporated using the S2 cell (G-030) setting. Transfected cells were maintained in six-well plates with 2 ml SF900 at 25°C for 48 h before imaging. For double stranded RNA treatment, transfected cells were treated with 10 µg of double stranded RNA added directly to the well immediately after electroporation and then again on day 3. Cells were then fixed on day 5. The following primers were used to generate DNA templates for T7 RNA synthesis reactions (Promega): CaM, 5′-AACGGCACAATTGACTTCC-3′, 5′-ACCGTCGC CATCGATATC-3′; AspN, 5′-GTGAGATCCTCGCTCAGTCC-3′, 5′-CATAGAGCTTGACGGAAGGC-3′; AspC, 5′-GGAAACAGCCAGA CTTCAGC-3′, 5′-GCTGTTGCAGGCAGATAACA-3′.

Immunostaining

S2 or *dSas4-; Jupiter::GFP* cells were allowed to adhere to coverslips coated with 0.5 mg/ml Concavalin A for 60 min in a covered 35-mm dish. Transfected S2 cells were fixed with 4% PFA diluted in PBS for 10 min. *dSas4-; Jupiter::GFP* cells were fixed with 0.25% glutaraldehyde diluted in PBS for 1 min, extracted for 1 min in Karsenti's buffer (80 mM Pipes, 1 mM $MgSO_4$, 5 mM EDTA, and 0.5% Triton X-100, pH 6.9), fixed again with 0.25% glutaraldehyde for 10 min, and then postfixed in $NaBH_4$ (1 mg/ml in H_2O) for 10 min. Cells were counterstained with DAPI for 1 min and then mounted in Vectashield (Vector Laboratories).

For brain staining, third-instar larvae were quickly dissected in SF900 media, and intact brains were transferred to 0.5-ml tubes containing SF900/0.5%BSA. Brains were fixed in 9% PFA/0.5% Triton X-100/SF900 with head-tail rotation for 30 min at room temperature. Brains were rinsed 3× in PBST (PBS and 0.1% Triton X-100) and then block-permeabilized in 1% BSA (wt/vol)/0.5% Triton X-100/PBS for 2 h at room temperature. Primary antibodies were diluted in 1% BSA (wt/vol)/0.5% Triton X-100/PBS and incubated overnight at 4°C. Brains were then washed three times in PBST for 10 min each at room temperature and were then incubated with secondary antibodies for 1 h at room temperature. After a 3× wash in PBST for 10 min, brains were counterstained with DAPI for 5 min and mounted in Aqua-Poly/Mount (Polysciences Inc.).

Antibodies

Antibodies included β-tubulin (1:250, E7; Developmental Studies Hybridoma Bank), PKC ζ (1:100, sc-216; Santa Cruz Biotechnology); centrosomin (1:500; Rusan Lab); phosphohistone H3 Ser10 (1:1,000, 06-570; EMD Millipore); FLAG (1:500, F1804; Sigma-Aldrich); and Deadpan (1:100, ab195172; Abcam). Secondary antibodies conjugated to Alexa Fluor 488, 568, and 647 were obtained from Life Technologies and used at 1:500.

Microscopy

All immunostaining and live-imaging experiments were performed on a Nikon Eclipse Ti–inverted microscope and imaged using a 10×/0.30 NA plan Fluor, 40×/1.30 NA plan Fluor, 100×/1.40 NA plan APO, or 100×/1.49 NA TIRF objective, CSU-22 spinning disc confocal module (Yokogawa), and either an ORCA-Flash4.0 CMOS (Hamamatsu) or interline transfer-cooled charge coupled device camera (CoolSNAP HQ2; Photometrics). 491-, 561-, and 642-nm solid-state lasers were used for excitation (VisiTech International), and a MAC6000 Automation Controller (Ludl Electronic Products) was used to operate an emission filter wheel equipped with Semrock Emission Filters. Metamorph software (v7.7.10; Molecular Devices) was used for image acquisition.

Live imaging

For live imaging of larval brains, we followed the method of Lerit et al. (2014) with the following modifications: brains were placed in a 50-µl drop of SF900 on a gas-permeable Lumox tissue culture dish (Sarstedt), and a coverslip was gently placed on top. Excess media was removed with a kimwipe until brains came in contact with the coverslip. A drop of halocarbon oil was then placed at each of the corners of the coverslip to prevent drift during imaging. For imaging in live S2 cells, cells were placed in a glass-bottom 35-mm tissue culture dish (MatTek) coated with 0.5 mg/ml Concavalin-A and allowed to adhere for 30–60 min before imaging.

For drug treatments, conditioned SF900 media was added to each dish to a final volume of 1 ml. An equal volume of a 2× solution of W-7 (400 µM in conditioned SF900 media, diluted from a 1 mM DMSO stock) was then gently but rapidly added to the dish and pipet mixed briefly to a final concentration of 200 µM W-7. Frames were acquired immediately after addition for the indicated time. All imaging was performed on a heated stage incubator set to 25°C.

Image and statistical analysis

Image analysis was performed using Fiji (Schindelin et al., 2012). Lateral pole distances were calculated by measuring the distance between the outermost kinetochore fibers at the pole. A cell was considered to have detached centrosomes if one or more centrosomes were positioned anywhere outside of the pole region. Colocalization analysis was performed using the plugin Coloc 2. Regions of interest were generated for each cell of interest, background subtracted (100 pixels), and analyzed using a point spread function of 3 and 10 Costes randomizations. Manual particle tracking was performed using the MTrackJ plugin (Meijering et al., 2012). Counting of NB number (deadpan staining of nuclei) and phosphohistoneH3Ser10-positive nuclei were performed using the cell counter plugin. Counts were restricted to clusters in the dorsal and ventral central brain region, as judged by MT staining. For kymograph analysis, images were acquired at a single confocal plane every 2–5 s for 2 min. To measure the flux rate for Asp and CaM, lines were drawn from the spindle midzone to the pole along the MT tracks and a kymograph generated using the "Reslice" plugin in Fiji. The flux rates of the speckles were determined from the slope of their movement on the kymograph. Statistical analysis and graph generation were performed with GraphPad Prism 6 software.

Adult brain size analysis

Age-matched females from each genotype were decapitated using a dissection needle. Forceps were used to remove the mouthparts, and heads were placed in a 1.5-ml microfuge tube filled with 8% PFA/SF900. Tubes were then placed in a shaking incubator set at 37°C and 250 rpm for at least 1 h. Samples were rinsed three times in PBS and further dissected by removing eyes and the remaining cuticle using forceps. Intact brains were placed on a stage micrometer slide under a Leica stereomicroscope outfitted with an IC80 HD camera (Leica) and captured. Measurements of brain width were performed in Fiji by drawing a straight line across the outermost tips of the optic lobes.

RNA extraction, cDNA synthesis, and quantitative PCR

For fly tissue, 10 pairs of ovaries from *yw* and asp^{C25}/Df adult females were dissected in triplicate in SF900 media and RNA extracted using 500 µl Trizol (Life Technologies). For tissue culture, ∼10^6 cells were pelleted at 2,500 *g* and homogenized in 500 µl Trizol. Samples were treated with Turbo-free DNase (Life Technologies), and 1 µg RNA was used for cDNA synthesis using the iScript cDNA synthesis kit (Bio-Rad). Quantitative PCR runs were performed on a Light Cycler 96 (Roche) using a two-step amplification protocol at 60°C with iQ SYBR Green Supermix (Bio-Rad) and 1 µl cDNA. Relative expression was calculated after the $\Delta\Delta C_t$ method using Rp49 primers as the normalizer. A paired *t* test was used to assess statistical significance based on three biological replicates per treatment. Asp and CaM primer sequences are available on request.

Online supplemental material

Fig. S1 shows *cam* and *asp* transcript levels via quantitative PCR after RNAi treatment for the experiment outlined in Fig. 1 (A and C), the effect of W-7 or control DMSO treatment on S2 cells expressing GFP-CaM and RFP-α-tubulin, and the pole focusing consequences after CaM and Asp loss in acentrosomal cells. Fig. S2 highlights the IQ motifs deleted to generate $Asp^{FL\Delta IQ}$, the ability of Asp^{FL} and $Asp^{FL\Delta IQ}$ to dimerize with Asp^{C} and the lack of stability for both Asp^{C} and Asp^{FL} after CaM depletion. Fig. S3 outlines the spindle pole localization for GFP-CaM in S2 cells. Fig. S4 shows the full panel from Fig. 7 D regarding spindle polarity establishment and maintenance, examples of both correct centrosome inheritance and GMC inheritance in asp^{T25} NBs, and analysis of NB number and mitotic cells in WT and mutant brains. Video 1 shows S2 cells expressing GFP-CaM and RFP-Asp. Video 2 shows mitotic NBs expressing GFP-CaM. Video 3 shows the same NB described in Video 2, but with the metaphase duration only to highlight streaming. Video 4 shows NB expressing asp^{FL}, asp^{N}, or $asp^{FL\Delta IQ}$. Video 5 shows NB from an asp^{t25}/Df mutant expressing tubulin-GFP. Video 6 shows NB from an asp^{t25}/Df mutant expressing tubulin-GFP. Video 7 shows NB from an asp^{t25}/Df mutant expressing Tubulin-GFP. Video 8 shows NB from an asp^{t25}/Df mutant expressing tubulin-GFP. Online supplemental material is available at http://www.jcb.org/cgi/content/full/jcb.201509054/DC1.

Acknowledgments

We thank members of the Rusan and A. Kelly Laboratories (National Cancer Institute, National Institutes of Health) for critical discussion and comments throughout this project. We thank K. Plevock for help with RNAi experiments, D. Lerit for critically reading of the manuscript, and C. Gonzalez for discussion and sharing reagents.

N.M. Rusan is supported by the Division of Intramural Research at the National Institutes of Health/National Heart, Lung, and Blood Institute (1ZIAHL006126).

The authors declare no competing financial interests.

Submitted: 11 September 2015
Accepted: 27 October 2015

References

Basto, R., J. Lau, T. Vinogradova, A. Gardiol, C.G. Woods, A. Khodjakov, and J.W. Raff. 2006. Flies without centrioles. *Cell.* 125:1375–1386. http://dx.doi.org/10.1016/j.cell.2006.05.025

Bond, J., E. Roberts, G.H. Mochida, D.J. Hampshire, S. Scott, J.M. Askham, K. Springell, M. Mahadevan, Y.J. Crow, A.F. Markham, et al. 2002. ASPM is a major determinant of cerebral cortical size. *Nat. Genet.* 32:316–320. http://dx.doi.org/10.1038/ng995

Bond, J., S. Scott, D.J. Hampshire, K. Springell, P. Corry, M.J. Abramowicz, G.H. Mochida, R.C.M. Hennekam, E.R. Maher, J.-P. Fryns, et al. 2003. Protein-truncating mutations in ASPM cause variable reduction in brain size. *Am. J. Hum. Genet.* 73:1170–1177. http://dx.doi.org/10.1086/379085

Bowman, S.K., R.A. Neumüller, M. Novatchkova, Q. Du, and J.A. Knoblich. 2006. The *Drosophila* NuMA homolog mud regulates spindle orientation in asymmetric cell division. *Dev. Cell.* 10:731–742. http://dx.doi.org/10.1016/j.devcel.2006.05.005

Carmena, M., C. Gonzalez, J. Casal, and P. Ripoll. 1991. Dosage dependence of maternal contribution to somatic cell division in *Drosophila* melanogaster. *Development.* 113:1357–1364.

Castellanos, E., P. Dominguez, and C. Gonzalez. 2008. Centrosome dysfunction in *Drosophila* neural stem cells causes tumors that are not due to genome instability. *Curr. Biol.* 18:1209–1214. http://dx.doi.org/10.1016/j.cub.2008.07.029

Conduit, P.T., and J.W. Raff. 2010. Cnn dynamics drive centrosome size asymmetry to ensure daughter centriole retention in *Drosophila* neuroblasts. *Curr. Biol.* 20:2187–2192. http://dx.doi.org/10.1016/j.cub.2010.11.055

Dionne, M.A., L. Howard, and D.A. Compton. 1999. NuMA is a component of an insoluble matrix at mitotic spindle poles. *Cell Motil. Cytoskeleton.* 42:189–203.http://dx.doi.org/10.1002/(SICI)1097-0169(1999)42:3<189::AID-CM3>3.0.CO;2-X

do Carmo Avides, M., and D.M. Glover. 1999. Abnormal spindle protein, Asp, and the integrity of mitotic centrosomal microtubule organizing centers. *Science.* 283:1733–1735. http://dx.doi.org/10.1126/science.283.5408.1733

Endow, S.A., R. Chandra, D.J. Komma, A.H. Yamamoto, and E.D. Salmon. 1994. Mutants of the *Drosophila* ncd microtubule motor protein cause centrosomal and spindle pole defects in mitosis. *J. Cell Sci.* 107:859–867.

Fish, J.L., Y. Kosodo, W. Enard, S. Pääbo, and W.B. Huttner. 2006. Aspm specifically maintains symmetric proliferative divisions of neuroepithelial cells. *Proc. Natl. Acad. Sci. USA.* 103:10438–10443. http://dx.doi.org/10.1073/pnas.0604066103

Franke, J.D., A.L. Boury, N.J. Gerald, and D.P. Kiehart. 2006. Native nonmuscle myosin II stability and light chain binding *in Drosophila melanogaster*. *Cell Motil. Cytoskeleton.* 63:604–622. http://dx.doi.org/10.1002/cm.20148

Gaglio, T., A. Saredi, J.B. Bingham, M.J. Hasbani, S.R. Gill, T.A. Schroer, and D.A. Compton. 1996. Opposing motor activities are required for the organization of the mammalian mitotic spindle pole. *J. Cell Biol.* 135:399–414. http://dx.doi.org/10.1083/jcb.135.2.399

Galletta, B.J., and N.M. Rusan. 2015. A yeast two-hybrid approach for probing protein–protein interactions at the centrosome. In Methods in Cell Biology. Vol. 129. B. Renata, and O. Karen, editors. Academic Press, Amsterdam. 251–277.

Galletta, B.J., R.X. Guillen, C.J. Fagerstrom, C.W. Brownlee, D.A. Lerit, T.L. Megraw, G.C. Rogers, and N.M. Rusan. 2014. *Drosophila* pericentrin requires interaction with calmodulin for its function at centrosomes and neuronal basal bodies but not at sperm basal bodies. *Mol. Biol. Cell.* 25:2682–2694. http://dx.doi.org/10.1091/mbc.E13-10-0617

Gonzalez, C., R.D. Saunders, J. Casal, I. Molina, M. Carmena, P. Ripoll, and D.M. Glover. 1990. Mutations at the asp locus of *Drosophila* lead to multiple free centrosomes in syncytial embryos, but restrict centrosome duplication in larval neuroblasts. *J. Cell Sci.* 96:605–616.

Goshima, G., and R.D. Vale. 2003. The roles of microtubule-based motor proteins in mitosis: comprehensive RNAi analysis in the *Drosophila* S2 cell line. *J. Cell Biol.* 162:1003–1016. http://dx.doi.org/10.1083/jcb.200303022

Goshima, G., R. Wollman, S.S. Goodwin, N. Zhang, J.M. Scholey, R.D. Vale, and N. Stuurman. 2007. Genes required for mitotic spindle assembly in Drosophila S2 cells. *Science.* 316:417–421. http://dx.doi.org/10.1126/science.1141314

Harborth, J., J. Wang, C. Gueth-Hallonet, K. Weber, and M. Osborn. 1999. Self assembly of NuMA: multiarm oligomers as structural units of a nuclear lattice. *EMBO J.* 18:1689–1700. http://dx.doi.org/10.1093/emboj/18.6.1689

Januschke, J., and C. Gonzalez. 2010. The interphase microtubule aster is a determinant of asymmetric division orientation in *Drosophila* neuroblasts. *J. Cell Biol.* 188:693–706. http://dx.doi.org/10.1083/jcb.200905024

Januschke, J., S. Llamazares, J. Reina, and C. Gonzalez. 2011. *Drosophila* neuroblasts retain the daughter centrosome. *Nat. Commun.* 2:243. http://dx.doi.org/10.1038/ncomms1245

Januschke, J., J. Reina, S. Llamazares, T. Bertran, F. Rossi, J. Roig, and C. Gonzalez. 2013. Centrobin controls mother-daughter centriole asymmetry in *Drosophila* neuroblasts. *Nat. Cell Biol.* 15:241–248. http://dx.doi.org/10.1038/ncb2671

Kisurina-Evgenieva, O., G. Mack, Q. Du, I. Macara, A. Khodjakov, and D.A. Compton. 2004. Multiple mechanisms regulate NuMA dynamics at spindle poles. *J. Cell Sci.* 117:6391–6400. http://dx.doi.org/10.1242/jcs.01568

Lecland, N., and J. Lüders. 2014. The dynamics of microtubule minus ends in the human mitotic spindle. *Nat. Cell Biol.* 16:770–778. http://dx.doi.org/10.1038/ncb2996

Lecland, N., A. Debec, A. Delmas, S. Moutinho-Pereira, N. Malmanche, A. Bouissou, C. Dupré, A. Jourdan, B. Raynaud-Messina, H. Maiato, and A. Guichet. 2013. Establishment and mitotic characterization of new *Drosophila* acentriolar cell lines from DSas-4 mutant. *Biol. Open.* 2:314–323. http://dx.doi.org/10.1242/bio.20133327

Lerit, D.A., and N.M. Rusan. 2013. PLP inhibits the activity of interphase centrosomes to ensure their proper segregation in stem cells. *J. Cell Biol.* 202:1013–1022. http://dx.doi.org/10.1083/jcb.201303141

Lerit, D.A., J.T. Smyth, and N.M. Rusan. 2013. Organelle asymmetry for proper fitness, function, and fate. *Chromosome Res.* 21:271–286. http://dx.doi.org/10.1007/s10577-013-9350-3

Lerit, D.A., K.M. Plevock, and N.M. Rusan. 2014. Live imaging of *Drosophila* larval neuroblasts. *J. Vis. Exp.* 89:e5175. http://dx.doi.org/10.3791/51756

Mahjoub, M.R., and T. Stearns. 2012. Supernumerary centrosomes nucleate extra cilia and compromise primary cilium signaling. *Curr. Biol.* 22:1628–1634. http://dx.doi.org/10.1016/j.cub.2012.06.057

Matos, I., A.J. Pereira, M. Lince-Faria, L.A. Cameron, E.D. Salmon, and H. Maiato. 2009. Synchronizing chromosome segregation by flux-dependent force equalization at kinetochores. *J. Cell Biol.* 186:11–26. http://dx.doi.org/10.1083/jcb.200904153

Matthies, H.J., H.B. McDonald, L.S. Goldstein, and W.E. Theurkauf. 1996. Anastral meiotic spindle morphogenesis: role of the non-claret disjunctional kinesin-like protein. *J. Cell Biol.* 134:455–464. http://dx.doi.org/10.1083/jcb.134.2.455

Meijering, E., O. Dzyubachyk, and I. Smal. 2012. Methods for cell and particle tracking. *Methods Enzymol.* 504:183–200. http://dx.doi.org/10.1016/B978-0-12-391857-4.00009-4

Merdes, A., K. Ramyar, J.D. Vechio, and D.W. Cleveland. 1996. A complex of NuMA and cytoplasmic dynein is essential for mitotic spindle assembly. *Cell.* 87:447–458. http://dx.doi.org/10.1016/S0092-8674(00)81365-3

Merdes, A., R. Heald, K. Samejima, W.C. Earnshaw, and D.W. Cleveland. 2000. Formation of spindle poles by dynein/dynactin-dependent transport of NuMA. *J. Cell Biol.* 149:851–862. http://dx.doi.org/10.1083/jcb.149.4.851

Morales-Mulia, S., and J.M. Scholey. 2005. Spindle pole organization in *Drosophila* S2 cells by dynein, abnormal spindle protein (Asp), and KLP10A. *Mol. Biol. Cell.* 16:3176–3186. http://dx.doi.org/10.1091/mbc.E04-12-1110

Morin, X., R. Daneman, M. Zavortink, and W. Chia. 2001. A protein trap strategy to detect GFP-tagged proteins expressed from their endogenous loci in *Drosophila*. *Proc. Natl. Acad. Sci. USA.* 98:15050–15055. http://dx.doi.org/10.1073/pnas.261408198

Osawa, M., M.B. Swindells, J. Tanikawa, T. Tanaka, T. Mase, T. Furuya, and M. Ikura. 1998. Solution structure of calmodulin-W-7 complex: the basis of diversity in molecular recognition. *J. Mol. Biol.* 276:165–176. http://dx.doi.org/10.1006/jmbi.1997.1524

Poulton, J.S., J.C. Cuningham, and M. Peifer. 2014. Acentrosomal *Drosophila* epithelial cells exhibit abnormal cell division, leading to cell death and compensatory proliferation. *Dev. Cell.* 30:731–745. http://dx.doi.org/10.1016/j.devcel.2014.08.007

Rath, U., G.C. Rogers, D. Tan, M.A. Gomez-Ferreria, D.W. Buster, H.J. Sosa, and D.J. Sharp. 2009. The *Drosophila* kinesin-13, KLP59D, impacts Pacman- and Flux-based chromosome movement. *Mol. Biol. Cell.* 20:4696–4705. http://dx.doi.org/10.1091/mbc.E09-07-0557

Rebollo, E., P. Sampaio, J. Januschke, S. Llamazares, H. Varmark, and C. González. 2007. Functionally unequal centrosomes drive spindle orientation in asymmetrically dividing *Drosophila* neural stem cells. *Dev. Cell.* 12:467–474. http://dx.doi.org/10.1016/j.devcel.2007.01.021

Riparbelli, M.G., G. Callaini, D.M. Glover, and Mdo.C. Avides. 2002. A requirement for the abnormal spindle protein to organise microtubules of the central spindle for cytokinesis in *Drosophila*. *J. Cell Sci.* 115:913–922.

Ripoll, P., S. Pimpinelli, M.M. Valdivia, and J. Avila. 1985. A cell division mutant of *Drosophila* with a functionally abnormal spindle. *Cell.* 41:907–912. http://dx.doi.org/10.1016/S0092-8674(85)80071-4

Rossignol, P., S. Collier, M. Bush, P. Shaw, and J.H. Doonan. 2007. Arabidopsis POT1A interacts with TERT-V(I8), an N-terminal splicing variant of telomerase. *J. Cell Sci.* 120:3678–3687. http://dx.doi.org/10.1242/jcs.004119

Rujano, M.A., L. Sanchez-Pulido, C. Pennetier, G. le Dez, and R. Basto. 2013. The microcephaly protein Asp regulates neuroepithelium morphogenesis by controlling the spatial distribution of myosin II. *Nat. Cell Biol.* 15:1294–1306. http://dx.doi.org/10.1038/ncb2858

Rusan, N.M., and M. Peifer. 2007. A role for a novel centrosome cycle in asymmetric cell division. *J. Cell Biol.* 177:13–20. http://dx.doi.org/10.1083/jcb.200612140

Saunders, R.D., M.C. Avides, T. Howard, C. Gonzalez, and D.M. Glover. 1997. The *Drosophila* gene abnormal spindle encodes a novel microtubule-associated protein that associates with the polar regions of the mitotic spindle. *J. Cell Biol.* 137:881–890. http://dx.doi.org/10.1083/jcb.137.4.881

Sawin, K.E., K. LeGuellec, M. Philippe, and T.J. Mitchison. 1992. Mitotic spindle organization by a plus-end-directed microtubule motor. *Nature.* 359:540–543. http://dx.doi.org/10.1038/359540a0

Schindelin, J., I. Arganda-Carreras, E. Frise, V. Kaynig, M. Longair, T. Pietzsch, S. Preibisch, C. Rueden, S. Saalfeld, B. Schmid, et al. 2012. Fiji: an open-source platform for biological-image analysis. *Nat. Methods.* 9:676–682. http://dx.doi.org/10.1038/nmeth.2019

Siegrist, S.E., and C.Q. Doe. 2006. Extrinsic cues orient the cell division axis in *Drosophila* embryonic neuroblasts. *Development.* 133:529–536. http://dx.doi.org/10.1242/dev.02211

Sir, J.-H., M. Pütz, O. Daly, C.G. Morrison, M. Dunning, J.V. Kilmartin, and F. Gergely. 2013. Loss of centrioles causes chromosomal instability in vertebrate somatic cells. *J. Cell Biol.* 203:747–756. http://dx.doi.org/10.1083/jcb.201309038

Trammell, M.A., N.M. Mahoney, D.A. Agard, and R.D. Vale. 2008. Mob4 plays a role in spindle focusing in *Drosophila* S2 cells. *J. Cell Sci.* 121:1284–1292. http://dx.doi.org/10.1242/jcs.017210

van der Voet, M., C.W.H. Berends, A. Perreault, T. Nguyen-Ngoc, P. Gönczy, M. Vidal, M. Boxem, and S. van den Heuvel. 2009. NuMA-related LIN-5, ASPM-1, calmodulin and dynein promote meiotic spindle rotation independently of cortical LIN-5/GPR/Galpha. *Nat. Cell Biol.* 11:269–277 (alpha). http://dx.doi.org/10.1038/ncb1834

Wakefield, J.G., S. Bonaccorsi, and M. Gatti. 2001. The *Drosophila* protein asp is involved in microtubule organization during spindle formation and cytokinesis. *J. Cell Biol.* 153:637–648. http://dx.doi.org/10.1083/jcb.153.4.637

Walczak, C.E., and R. Heald. 2008. Mechanisms of mitotic spindle assembly and function. In International Review of Cytology. Vol. 265. W.J. Kwang, editor. Academic Press, Amsterdam. 111–158.

Welsh, M.J., J.R. Dedman, B.R. Brinkley, and A.R. Means. 1978. Calcium-dependent regulator protein: localization in mitotic apparatus of eukaryotic cells. *Proc. Natl. Acad. Sci. USA.* 75:1867–1871. http://dx.doi.org/10.1073/pnas.75.4.1867

Xu, X.-L., W. Ma, Y.-B. Zhu, C. Wang, B.-Y. Wang, N. An, L. An, Y. Liu, Z.-H. Wu, and J.-H. Tian. 2012. The microtubule-associated protein ASPM regulates spindle assembly and meiotic progression in mouse oocytes. *PLoS One.* 7:e49303. http://dx.doi.org/10.1371/journal.pone.0049303